IEEE Access
Multidisciplinary | Rapid Review | Open Access Journal

Received 8 May 2024, accepted 4 June 2024, date of publication 10 June 2024, date of current version 17 June 2024.

Digital Object Identifier 10.1109/ACCESS.2024.3411592

METHODS

High-Relative-Bandwidth Multiband LNA Distortion Elimination With Neural Network

ZHENG XIANG LI AND RUI LV
State Key Laboratory of Media Convergence and Communication, Communication University of China, Beijing 100024, China
Corresponding author: Zheng Xiang Li (lizhengxiang@cuc.edu.cn)

This work was supported in part by the Fundamental Research Funds for the Central Universities.

ABSTRACT This article presents an innovative approach that harnesses neural networks (NN) to eliminate non-linear distortion in low-noise amplifier (LNA) within multi-channel direct sampling receivers (MDSR). Current mainstream methods, such as those relying on memory polynomial or Volterra models, face challenges in effectively addressing the demand for LNA linearization modeling, particularly in scenarios with high fractional bandwidth and stochastic inputs. The proposed method incorporates two key technologies to support NN. First, using input signals with specific frequency properties to derive ground truth values by isolating distortion components from the LNA output signals in the frequency domain, simplifies the process of acquiring training samples and enhances accuracy. Additionally, by utilizing mathematical characteristics of LNA output signals, such as instantaneous rate of change, magnitude, and non-uniformly sampled memory points, it performs feature engineering to simultaneously reduce the complexity of the NN and enhance its generalization capabilities. Evaluation with the LNA (ZFL-500LN+) demonstrates outstanding performance in suppressing multiple harmonics and inter-modulation components, which approaches the quantization noise floor of the analog-to-digital converter, especially harmonic reduction of up to 46 dB in the worst distorted channel. These results show the potential of this method to enhance the performance of MDSR.

INDEX TERMS LNA, NN, non-linear distortion, multiband receivers, high fractional bandwidth, distortion elimination.

I. INTRODUCTION

In numerous communication systems, there is a need to employ a receiving system that can simultaneously capture multiple channels of radio signals. For instance, in the field of shortwave communication applications, it is feasible to utilize a single analog-to-digital converter (ADC) to directly acquire all the channels within the entire 30MHz communication bandwidth. Direct RF-sampling receivers are receiver architectures that directly sample the RF signal without the need for intermediate frequency (IF) or base-band converters. This architecture offers a higher level of integration by reducing active signal chain components and supporting elements such as different local oscillators and intermediate frequency band-pass filters. As the communications industry shifts towards multi-band multi-channel radios, the direct RF-sampling architecture is gaining even more support, as it enables the transition from one heterodyne receiver per band to one RF-sampling ADC per radio [1]. LNAs play a critical role in radio receiver performance. The success of a receiver's design is measured in various dimensions, including receiver sensitivity and selectivity. RF design engineers work to optimize the receiver's front-end performance, with a particular focus on the first active component [2].

Fractional bandwidth (FBW) is a term used in communication engineering to describe the bandwidth of a signal relative to its center frequency. It is a measure of the range of frequencies that a signal occupies in relation to its center frequency. FBW is an important parameter for a variety of applications in communication systems, In practice, the nonlinear characteristics of the amplifier are directly related to the FBW. When the FBW is low, amplifier can simply

The associate editor cordinating the review of this manuscript and approving it for publication was Fabian Khateb.

consider the nonlinear static characteristics. As the FBW increases, the memory effect of the amplifier becomes more pronounced. Specifically, when the FBW exceeds 100%, nonlinearity primarily induced by memory effects due to frequency selectivity becomes significantly noticeable after approximately one octave. In multi-band receivers such as shortwave full-band (3∼30MHz) direct acquisition applications, LNA needs to face a large FBW close to 160%, which is a great challenge for its linearization.

When direct RF-sampling receivers operate in multi-channel mode, such as when receiving the entire HF signal frequency range (3∼30 MHz), they allow for the simultaneous reception of multiple channels with different signal modulation and power levels. However, this application inevitably presents certain challenges. As the total RF signal power from the antenna approaches the gain compression point of the LNA, it ceases to operate in the linear region and enters the non-linear region. The LNA saturates and partially works in the non-linear regime, resulting in the generation of non-linear distortions in high-energy channels [3], [4], [5]. These distortions not only degrade the signal quality of nearby channels but also interfere with and drown out weak signals by harmonics and intermodulation components of strong signals. While this problem can be addressed in traditional single-channel reception by using pre-select band-pass filters, it becomes challenging in multi-channel or full-frequency-range reception scenarios. Therefore, it is imperative to employ appropriate and effective compensation methods to address this issue.

To address the impact of LNA nonlinearity, numerous studies have been conducted. One common approach is the nonlinear segmented calibration approach, which divides uncalibrated data into different segments and applies linearization to each segment to enhance calibration accuracy. Previous studies [6], [7] have utilized this method because of its potential for achieving high accuracy, although it heavily relies on the expertise of the calibrator. Another method proposed by Zhou et al. [8] involves using Discrete Fourier Transform (DFT) to determine these segments. However, this approach requires substantial effort in segmenting data and primarily focuses on single-channel input measurements rather than simultaneous multi-channel input calibration. A receiver distortion suppression method is proposed in the literature [9], which addresses the joint mitigation of nonlinear RF and baseband distortions in the RF front-end of Direct-Conversion Receivers (DCR). The article uses multi-level memoryless polynomials for effective mitigation. In order to avoid the nonlinearity caused by the in-band radio frequency simulation part of a single frequency band, the article proposes a method of using multiple sets of coefficients (called AF) when changing the center frequency to support frequency-selective nature (memory) of associated nonlinearities when changing the center frequency. From the methods and test parameters used in the article, it can be analyzed that the paper targets signals with low FBW (<13%), so that the memory effect of the device can be ignored. However, for high FBW, nonlinearity is obviously affected by memory application scenarios, this approach cannot meet the requirements. An alternative solution proposed in [10] is based on Lookup Tables (LUT). It acquires the nonlinear parameters of the LNA to determine the LUT parameters and corrects the received data using the LUT during reception. However, this solution assumes uniform characteristics of the LNA across the entire operating frequency range, which is challenging to ensure. It also overlooks the fact that the LNA functions as a nonlinear dynamic system, and memoryless nonlinear correction may only be suitable for narrowband signals [11]. The reference channel method, extensively researched in numerous studies [5], [12], [13], [14], [15], involves using a reference receiver (Rx_ref) auxiliary ADC to sample the input signal before it reaches the LNA. By employing algorithms to estimate distortion, the impact of LNA nonlinearity can be reduced to some extent in the primary receiver channel. However, it is crucial to consider real-time variations in calibration and correction parameters caused by strong signals. Additionally, this solution requires the addition of an extra ADC path, leading to increased equipment costs and complexity. The statistical properties of the frequency and total power level of received signals cannot be known or predetermined in advance. Analyzing the nonlinear behavior of LNA with multiple strong signals received in different channels using traditional models like Volterra and Hammerstein, which are designed for analyzing single-channel signals [16], becomes complex and challenging, especially when considering the memory effect of LNA.

Backpropagation NN demonstrate efficacy in conducting input-driven nonlinear modeling by leveraging multi-layered architectures and the iterative optimization facilitated by the backpropagation algorithm, allowing for the extraction of intricate features and patterns from data. In the context of applying NN to amplifier linearization, most studies [17], [18], [19], [20], [21], [22] have primarily focused on using Digital Predistortion (DPD) in power amplifiers. In the application of DPD, the encountered signals exhibit stable time-domain or frequency-domain statistical characteristics, such as relatively fixed center frequencies, bandwidths, and power levels. The correction is primarily targeted at signals with a 1dB compression point level, addressing the conditions of significant distortion. Moreover, there is a greater focus on odd-order harmonics affecting the in-band performance. Based on these premises, the DPD algorithm typically perform statistical compensation for distortions where the probability distribution is generally stationary. However, for LNAs in multi-frequency band reception, both the frequency-domain and time-domain inputs are stochastic. Signals and interference with varying intensities amplitudes and bandwidths within the band exhibit unstable statistical probability distributions. Additionally, not only odd-order but also even-order harmonics are equally important to consider. The superposition of these signals causing LNA distortion also

lacks statistical significance. Therefore, it is necessary to find a model that is dynamically correlated with the real-time state of the input signals rather than statistically similar to address this challenge.

In this paper, a NN-based method is proposed for eliminating nonlinear components in LNA. Firstly, theoretical and experimental research on the characteristics of LNAs was conducted, and it was confirmed that LNA nonlinearity is not only dependent on the total power level but also related to its frequency distribution [23] and exhibits a certain memory effect. To address these challenges, Significant effort was invested in studying the input signal characteristics related to the inherent properties of LNAs, and theoretical analysis and experiments were conducted. The results were surprisingly positive. A novel approach, focusing on input-driven models to address the issue of LNA linearization, is presented as a part of NN. This approach integrates real-time signal analysis and various dimensions of LNA characteristics with the implementation of a NN. It requires minimal computational resources and achieves excellent distortion compensation results. Ultimately, the harmonic components of the compensated output samples are significantly reduced to the level of background noise. Our contributions are summarized as follows:

- Multiple sets of single-tone and two-tone signals with varying frequencies and amplitudes were employed to stimulate the LNA and collect distortion response samples. Subsequently, these samples were used to train a NN for building an input-driven LNA distortion model.
- A Method for Acquiring Ground Truth is proposed: An approach for obtaining ground truth was developed, involving using the output of the LNA when excited with known signals as training data and then reconstructing the initial exciting signals as the ground truth. This method eliminates the need to collect distortion-free input signals as a reference, simplifying the process of acquiring training samples.

A study was conducted to explore mathematical features capturing the correlation between input signals and LNA characteristics. These features were used as inputs for the NN, thereby reducing the network's complexity and enhancing the model's generalization capability.

II. AMPLIFIER DISTORTION ANALYSES

LNA typically operate in Class A, as illustrated in figure 1. The bias point (Q) is strategically positioned near the center of the device's maximum current and voltage capabilities to extend the linear working dynamic range. Distortion levels are predominantly influenced by the operational range, as depicted in the figure 1. The static operating point of a Class A amplifier is carefully placed within the central region to ensure linearity. Consequently, when the reception signal is weak, the amplifier exhibits relatively low distortion and accurately amplifies the signal. As the dynamic range of the input signal gradually increases, along with the rise in signal

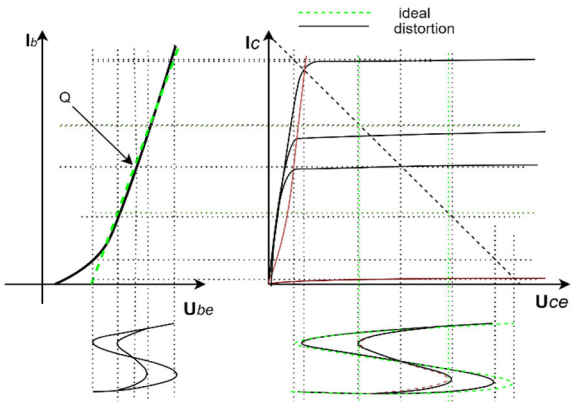

FIGURE 1. Ideal and distortion of amplifier. Magnetization as a function.

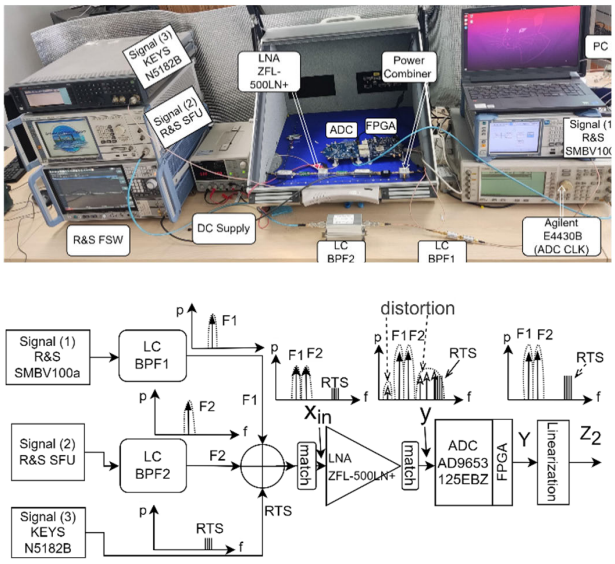

FIGURE 2. Experimental platform setups and block diagram.

amplitude, the positive half-cycle of the signal may enter the amplifier's saturation region, while the negative half-cycle signal approaches the cutoff region, resulting in distortion increase.

After experiments, it became evident that the distortion characteristics of the positive half-cycle and the negative half-cycle of the signal were not entirely consistent. This suggests that when a larger signal passes through the LNA, the positive and negative half-cycles of the output signal become unbalanced. Consequently, the use of the Volterra method is not suitable [24]. In the following sections, The relationship characteristics between the LNA's distortion-free output (the method for obtaining distortion-free signals will be provided later) and the actual output signal (with distortion) will be measured.

The experimental hardware platform system is illustrated in figure 2. Three different experiments are accomplished through configuration. During the testing of LNA characteristics and the acquisition of NN training parameter sets,

the switching between single-tone F1 or two-tone [F1, F2] is achieved by controlling the enablement of the two signal source outputs at the front end. To ensure ideal conditions during the testing process, corresponding LC filters at the respective frequencies are employed to filter the signals, ensuring that the harmonics of F1 and F2 are below −100dBc. Without considering the passive intermodulation (PIM) parameters of the power combiner, it is regarded as a distortion-free two-tone signal. In the final system testing phase, [F1, F2] represents analog distortion-free strong signals generated by the vector source, while RTS (receiving target signal) simulates a weak target signal. Due to RTS lower output amplitude, harmonic distortion issues of the device were not considered. Please note that the typical gain of the ZFL-500LN+ module within the 3-30MHz range is 27dB. However, during the testing process, it was noticed that both the input and output impedances of the module deviated from the desired 50Ω. To address this impedance mismatch, resistive matching networks were applied at both the input and output, resulting in a total loss of 6dB. Furthermore, an output power splitter introduced an additional 3dB loss. As a result, for the measurement platform, the effective front-end gain was reduced to 18dB.

The test signal Xin after passing through the Bandpass Filter (BPF) can be regarded as a composition of noise $n_x(t)$ and an undistorted single-tone signal with amplitude A, as illustrated in the following formula.

$$Xin(t) = A\sin wt + nx(t) \tag{1}$$

When X_{in} serves as the input to the LNA, it results in the signal Y, which incorporates the amplified X_{in} by a factor of a. The gain, denoted as a, introduces noise random variables $NF_{lna}(t)$ generated by the LNA, along with harmonic distortion components $f_{dis}(X_{in})$.

$$Y(t) = a \times A\sin wt + a \times nx(t) + NFlna(t) + fdis(Xin) \tag{2}$$

$Y(t)$ is the out-sampling sequence for the ADC, $Y = \{$y[t], y[t-1], y[t-2], …y[t-k]$\}$, where k is the maximum depth of samples to be stored. In this context, $f_{dis}(X_{in})$ represents the harmonic components of the signal after passing through the LNA, excluding the fundamental frequency. As the test signal X_e is a known signal, it is easy to implement $F_{gt}()$, which allows harmonic removal processing, resulting in X_e. This, in turn, leads to the generation of Ground Truth (GT) sets used for training, with the specific methodology detailed in the subsequent subsection.

$$Xe(t) = \text{Fgt}(Y) = a \times A\sin wt + a \times nx(t) + NFlna(t) \tag{3}$$

Thus, the difference between the LNA output and the ideal output is represented as the distortion component of the amplifier.

$$D(t) = (Y - Xe) = fdis(Xin) \tag{4}$$

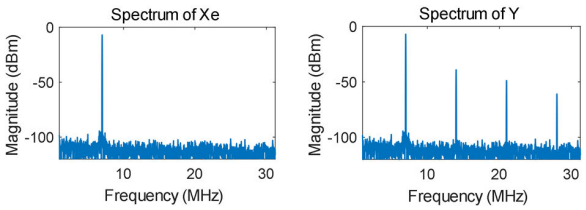

FIGURE 3. Spectra of X_e (without harmonic distortion) and Y (with harmonic distortion) for test.

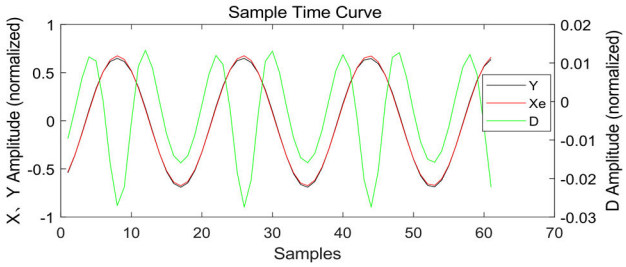

FIGURE 4. X_e, Y and D time-domain waveform curve.

Utilizing the test system show in Figure 2, activate signal source (1) while deactivating signal sources (2) and (3). At this point, X_{in} is a single-tone signal. Under the assumption that the LNA introduces only signal gain and distortion, consider X_e as our desired ideal output. If the gain is normalized to 1, It can utilize X_e as the input signal X_{in}, in conjunction with Y, to study the characteristics of the amplifier. Subsequently, the distortion characteristics of the LNA are analyzed using X_e and Y.

The next step test involves using a 7MHz sinusoidal test input, with a power level of -21dBm. At this point, it close to the 1dB input compression point (−19dBm) of the LNA (ZFL-500LN+). From the spectrum of Y shown in Figure 3, it shows that the LNA output has a component at 7MHz (plotted as 6.99615) with a power level of −7.0dBm. The second harmonic at 14MHz (plotted as 13.9999) has a power level of −39.1dBm, and the third harmonic at 21MHz (plotted as 21.0114) has a power level of −51.3 dBm. Therefore, at this point, the LNA's HD2 is 32.1 dBc, and HD3 is 44.3 dBc. After removing the harmonics, X_e is obtained, serving as the basis for the following tests. The spectra of X_e and Y are shown in the Figure 3.

A. TEST ONE

X_e and Y time-domain waveform testing. Along with the display of their errors, as depicted in Figure 4. The red curve represents X_e, while the black curve represents Y. When normalized for gain, it is observed that the curves do not coincide. This discrepancy is attributed to the presence of distortion in the LNA output. The error term, denoted as D in green, represents the distortion component (as a constant amplification factor was applied for observation). From the graph, it is evident that the amplifier's distortion characteristics are not symmetrical between the positive and negative half-cycles (the distortion is not symmetric). Furthermore,

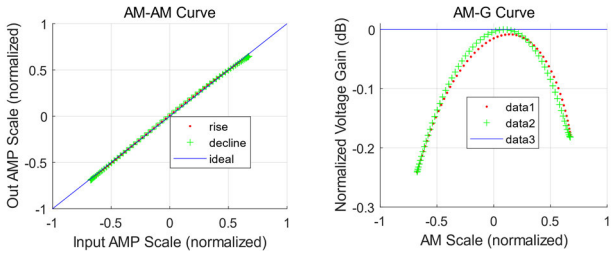

FIGURE 5. AM-AM and AM-G curves.

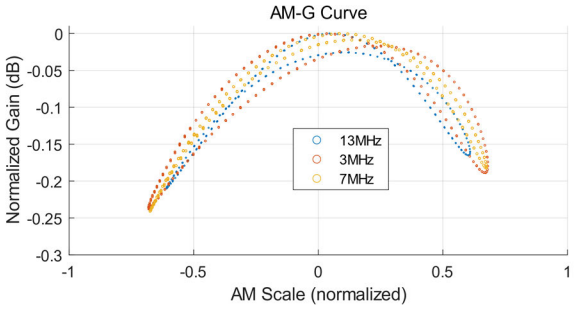

FIGURE 6. AM-G Curves at different frequencies.

it was observed that the distortion during the rising and falling phases is also not strictly symmetrical.

B. TEST TWO

As shown in figure 5, The AM-AM curves of X_e and Y were obtained after normalization. In the curve, the red portion represents signal levels during the rising phase, while the green portion represents signal levels during the falling phase. From the AM-AM curve, it is evident that observing distortion is challenging when absolute distortion is minimal. Therefore, an alternative method was adopted, as illustrated in figure 5. The AM-G curve represents the logarithmic relationship between the amplifier's operational level and the amplifier gain. This method offers an intuitive means of visualizing LNA distortion under low-distortion conditions. In the ideal scenario of a distortion-free amplifier, the curve should be a horizontal line. However, in practical situations, LNA gain varies with changes in signal amplitude. It exhibits higher gain in the middle (for lower power signals) compared to the edges (for higher power signals). Additionally, under the same signal intensity, differences in gain may arise due to variations in signal frequency and the phase of the signal, which aligns with the conclusions drawn from the first experiment.

C. TEST THREE

Tests were conducted at multiple frequencies (3MHz, 7MHz, 13MHz) at similar power levels to examine the AM-G curves of the LNA, as shown in figure 6. It is evident that the amplifier gain curves exhibit similar trends but are not identical. This reflects that the amplifier's distortion characteristics are not coincide when operating under different frequency. This inconsistency cannot be overlooked, especially when stringent distortion correction requirements are in place.

From the above experiments, conclusions about the amplifier core and matching circuits can be drawn when the LNA operates within a wide dynamic range, treating them as a holistic 'black box':

- The amplification distortion in the positive and negative half-cycles of the output waveform is inconsistent.
- The gain characteristics of the amplifier during signal level transitions (rising and falling phases) are also inconsistent.
- When operating at different frequencies, the gain characteristics exhibit similar trends but with variations.

Therefore, when considering distortion correction, the above parameter characteristics need to be taken into account as contributing factors to LNA distortion. Based on the experimental results and discussions mentioned above, our future work will focus on investigating methods to eliminate the distortion introduced by the LNA.

III. GROUND TRUTH IMPLEMENTATION

During the training phase of the NNmodel using known signals, to measure the distortion component of the amplifier output $f_{dis}(X_{in})$, it is essential to obtain the ground truth sample X_e under the assumption of the amplifier's ideal conditions. The method for obtaining X_e is denoted as the paradigm $F_{gt}()$.In this section, we will discuss two implementation methods for $F_{gt}()$, with the second method being the latest proposition in this paper.

A. METHOD 1

The approach employed is in line with various pre-distortion-related literature. It involves the synchronous collection of signals X_{in} and output Y before entering the amplifier. Subsequently, X_{in} and Y undergo delay and power alignment. Power alignment includes adjusting X_{in} with a fixed gain (gr) to ensure consistent power amplitudes between X_{in} and Y.

$$F_{gt}(Xin(t)) = Xe(t) = \mathrm{gr} \times Xin(t) \tag{5}$$

$$D(t) = Y(t) - \mathrm{gr} \times Xin(t) \tag{6}$$

The value of gr can be determined through various methods; for example, it employ power averaging as shown in equation (7) of gr, while other methods are not discussed here. In this case, the mean square error of the amplifier's distortion component D is Ed within one calculation cycle. The parameter $a(f)$ in equation (7) denotes the practical gain of the amplifier, and when the amplifier operates within a broad bandwidth, it manifests as a variable value dependent on the frequency rather than a constant.

$$Ed = \sum_{t=1}^{n}((a(f) - gr)A\sin wt + (a(f) - gr)nx(t) + NFlna(t))^2$$

where

$$\mathrm{gr} = \sqrt{\sum_t Y(t)^2 \div \sum_t Xin(t)^2} \tag{7}$$

B. METHOD 2

Since the test signals are simple and known (single-tone or two-tone), reconstruction in the digital domain is possible. Literature sources [24] employed parameter fitting methods, but these fitting techniques introduce additional errors due to issues such as noise component estimation, measurement interference, and errors in recovering carrier frequency, amplitude, and phase. This paper proposes a novel method with the fundamental idea of removing intermodulation and harmonic components in the frequency domain. Nonlinear distortion is more easily discernible in the frequency domain. If signals with clear independent distribution characteristics between signals and distortion in the frequency domain are used as a training set (such as pure tones or dual tones), it becomes easy to identify and separate ideal signals from nonlinear distortion components in the frequency domain using a simple algorithm, much like distinguishing black beans from white beans in a pile of beans. The specific method $F_{gt}()$ to get X_e from $\boldsymbol{Y}$ is outlined as follows:

- Apply windowing to $\boldsymbol{Y}$ to obtain $\boldsymbol{Y}_w = \boldsymbol{Y} \cdot \boldsymbol{W}$, where $\boldsymbol{W}$ represents the window.
- Perform FFT transformation on $\boldsymbol{Y}_w$ to obtain the frequency domain $\boldsymbol{Y_f} = \text{FFT}(\boldsymbol{Y}_w)$.
- Measure the horizontal index of the main frequency component in $\boldsymbol{Y_f}$ and calculate the indices of its harmonic and intermodulation components. Replace the components at the harmonic indices with the noise values of the surrounding n indices, resulting in $\boldsymbol{Y_{fr}} = \text{RH}(\boldsymbol{Y_f})$.
- Apply IFFT to $\boldsymbol{Y_{fr}}$ to obtain the time-domain waveform $\boldsymbol{Y_r} = \text{IFFT}(\boldsymbol{Y_{fr}})$.
- Obtain X_e by dividing $\boldsymbol{Y_r}$ by the window $\boldsymbol{X_e} = Y_r / \boldsymbol{W}$.

This method aims to minimize the errors introduced by parameter fitting by eliminating harmonic and inter modulation components in the frequency domain.

By employing the methods described above to obtain X_e, considering that the window function W has relatively small amplitudes at the ends in the time domain (approaching zero), data truncation is performed, removing the initial and final data. Only the central section is utilized to enhance precision.

Error Analysis: From the above processes, it is evident that applying windowing and de-windowing, as well as FFT and IFFT operations (with a length of N_{fft}), introduce negligible computational errors. The primary source of error in the entire process arises from RH() in step 3. However, because replace the components at the harmonic indices with the noise values of the surrounding n indices, the error can be controlled within the level of the quantization noise floor.

$$Ed = \sum_{t=1}^{n} (nx(t) + Flna(t))^2 \times ratio$$

where

$$ratio = (n/\text{Nfft}) < 1 \tag{8}$$

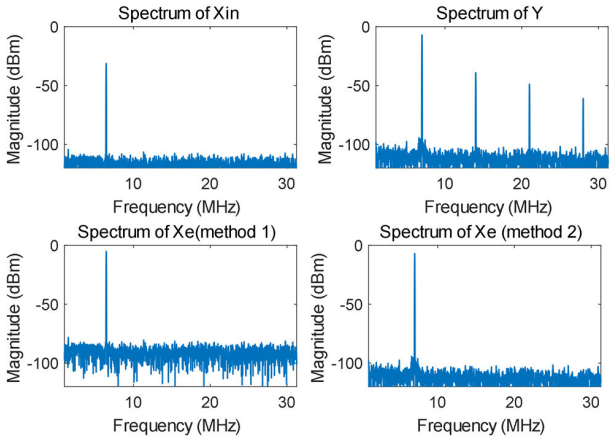

FIGURE 7. Spectra of Xin, Y and Xe(method1), Xe (method2).

In the equation (8), represents the ratio of the total number of points replaced, which accumulates around n indices at the harmonic frequency points, relative to the total number of FFT points. It can be observed from equations (5) and (6) that Ed in Method 2 is smaller than in Method 1. Furthermore, Method 2 eliminates the need to obtain Xin, simplifying the process of acquiring training samples. In this paper, this method is utilized to achieve the functionality of Fgt

IV. THE PROPOSED CALIBRATION SCHEME

In this section, a uniform generic regression neural network is introduced to address the LNA distortion issues discussed earlier. As mentioned in the previous section, when the LNA amplification characteristics differ in different feature dimensions of the input signal, this paper considers two dimensions: power level and frequency. The system structure is shown in figure 8, and the system operation primarily involves three main components: feature engineering, NN network, and training engine.

During the experimental process, challenges were encountered in using a single, simple NN structure to learn LNA device distortion characteristics in the time domain across different dimensions. After extensive research, it was decided to address high-frequency distortion and low-frequency distortion separately by employing two simple NN in a cascaded manner. The corresponding system structure, NN training, and signal correction processes are divided into two parts: P1 (Part 1) and P2 (Part 2). First, the distortion correction for LNA harmonics and inter-modulation frequencies higher than the fundamental

frequency is completed, corresponding to the training of NN_{P1} Then, $NN_{P1}()$ is used to assist in the training of P2, achieving distortion correction for LNA inter-modulation frequencies lower than the fundamental frequency.

Although the NN training and signal correction processes are split into two parts, each part has its own independent NN that serves a slightly different function. However, the structures of the two parts are similar, with differences in NN

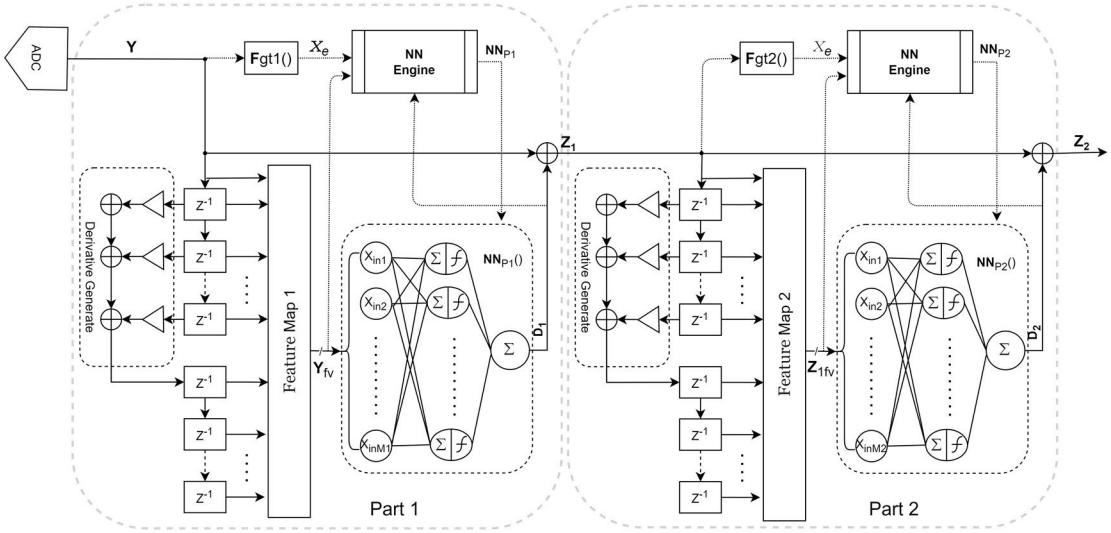

FIGURE 8. Distortion correction system principal diagram.

hyper-parameters and network parameters. This facilitates module reuse during the development and implementation.

A. NN FEATURE ENGINEERING

In NN, the inputs are feature vectors. To achieve real-time processing in an embedded manner (FPGA), it is essential to use as few neurons as possible for computations. Shallow NN typically have limited capacity, and therefore, feature vectors need to adequately represent the key information in the input data to minimize the complexity of the model. Effective feature vectors can assist the model in better capturing patterns and structures in the data, thereby enhancing the model's performance. If the feature vectors capture the essential features of the data while keeping the model simple, they can utilize the input data's information fully, making it easier for the model to learn and generalize.

In the preceding sections of this paper, the diverse characteristics of LNA at different frequencies and power levels were examined. In the subsequent sections, three main types of feature data extracted from input waveforms are predominantly utilized. The specific feature vectors are derived from current and delayed data, as well as current gradients and gradient-delayed gradient data. The Feature Map module selects these feature vectors, which are then fed into the input layer of the NN.

1) FEATURE VECTOR A: SAMPLE POINTS

Directly sampled, the amplitude dimension information of the current signal is represented by feature vector A. Its length is DelayStep1N. Taking into account the memory effects displayed by the amplifier, in Part A of the NN section, the input features for the NN consist of the five previously sampled points before the current one. In Part B, DelayStep1N = 1 is employed.

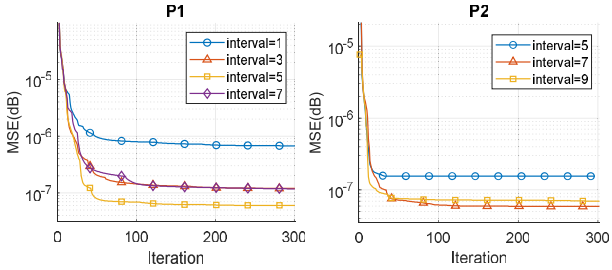

FIGURE 9. Model training performance for interval values of P1 and P2.

2) FEATURE VECTOR B: EXTRACTED SAMPLE POINTS

In this design, the ADC sampling rate is 125MHz, and the target sampling frequency range is the shortwave frequency range of 3∼30MHz, which falls into the oversampling state. The objective is to provide the NN with an extended observation period while maintaining low complexity for increased memory depth. In Part P1, a uniform sampling is conducted at interval points between 5 sequentially sampled data points. A total of Interval_N = 5 extracted sample points are used. The selection of interval values, as depicted in figure 9, has been determined through experimentation, with interval = 5 yielding the best model training convergence speed and accuracy. Part P2 follows the same methodology to obtain the optimal hyperparameters.

3) FEATURE VECTOR C: GRADIENT OF SAMPLE POINTS

Derivatives serve as a potent tool for elucidating the dynamic attributes of signals, as they contain gradient value information at sampled points, providing various insights into the signal. First-order derivatives at each sample point reflect the rate of change of the signal at that point. This implies that instantaneous changes in the signal can be accurately captured, as the magnitude of the first derivative represents the

slope or rate of change of the signal. When the magnitude of the first derivative is substantial, it indicates that the signal has undergone significant fluctuations in the vicinity of that point, which is crucial for high-frequency signal analysis. Second-order derivatives provide information about the curvature and rate of change of the signal.

$$\frac{\partial Xin(t)}{\partial t} = Aw \times \cos wt + \frac{\partial nx(t)}{\partial t}$$
$$\frac{\partial^2 Xin(t)}{\partial^2 t} = Aw^2 \times \sin wt + \frac{\partial^2 nx(t)}{\partial^2 t} \quad (9)$$

From equations (9), it can be observed that computing the first and second derivatives results in amplitude terms in the expressions. This implies that by taking derivatives of the signal, information related to the instantaneous frequency dimension of the current signal is indirectly acquired. In the implementation process, a structure similar to FIR (Finite Impulse Response) is utilized to obtain the derivative sequence of the input sequence [23]. In a physical sense, the derivative at a particular point signifies the magnitude and rate of change of the signal at that point. A larger absolute value of the derivative indicates rapid and significant changes at that point, which naturally corresponds to higher instantaneous frequencies and larger high-frequency components.

B. TRAINING AND INFERENCE

In this section, the work is divided into two phases, as described earlier. The first phase of training primarily uses feature signals to train the NN, enabling it to capture the characteristics of the LNA. The second phase involves the utilization of the learned LNA properties to process unknown real-world signals and remove the inter-modulation and distortion introduced by the LNA. Below, a detailed overview of the specific tasks in each of these phases is provided.

1) TRAINING PHASE

The training system employed is illustrated in figure 8. Known single-tone and two-tone signals with different frequencies and amplitudes generated by a signal source serve as the training samples to train the NN. During the training process, the NN learns the distortion characteristics of the LNA under different signal dimensions, resulting in the corresponding NN model for the LNA device. In the experiments, addressing the distortion characteristics of the LNA device using a simple NN proved to be challenging. Therefore, the training process is divided into two stages to handle the removal of high-frequency distortion and low-frequency distortion. In the first stage (P1), the training of NN1($\mathrm{NN_{P1}}$) is conducted to correct distortion related to harmonics and inter-modulation frequencies higher than the fundamental frequency. Then, $\mathrm{NN_{P1}}()$ is used to assist in the training of NN2 ($\mathrm{NN_{P2}}$), which focuses on the correction of distortion components with frequencies lower than the fundamental frequency.

P1's NN individual training utilizes single-tone signals, and its characteristic is that all distortion signal frequency components are higher than the fundamental component. In the time domain, this is reflected as the distortion component's period being shorter than that of the fundamental component, making it possible to generate $f_{dis}(X_{in})$ with a relatively short memory time length in the time domain correction. The corresponding GT sample signal distortion removal method for P1 mainly involves eliminating multiple harmonics of single-tone signals, such as the 2nd, 3rd, 4th, etc. Utilizing Y and the GT samples, the ultimate training of the NN is denoted as $\mathrm{NN_{P1}}$.

$\mathrm{P_1}$'s NN undergoes independent training using single-tone signals, with the characteristic that all distortion signal frequency components are higher than the fundamental component. In the time domain, this is manifested by the distortion component having a shorter period than that of the fundamental component, enabling the generation of $f_{dis}(X_{in})$ with a relatively short memory time length in time domain correction. The corresponding GT distortion-free sample signal for $\mathrm{P_1}$ is obtained using $F_{\mathrm{gt1}}()$, following the method outlined in Section III-*B*, where the distortion removal technique RH() primarily involves eliminating multiple harmonics of single-tone signals, such as the 2nd, 3rd, 4th, and so on. By utilizing Y and GT samples, ultimate training of the NN is denoted as $\mathrm{NN_{P1}}$. The 'NN Engines' of P1 in figure 8 represent the training program modules used for training NNP1.

The final Inference output of P1 is denoted as Z_1, as shown in figure 8. Here, Y_{fv} represents Y after feature extraction, which is sent to the NN as the feature vector. P2 focuses on correcting distortion with inter-modulation frequencies lower than the fundamental frequency. In this section, NN training employs two-tone signals [F1, F2]. The two-tone signals are first Inference through $\mathrm{NN_{P1}}$ to obtain Z1, which, in turn, serves as the input for P2 after feature extraction, resulting in the feature vector $\mathrm{Z_{1fv}}$. $\mathrm{Z_1}$ is then processed to obtain the corresponding training GT sample by $F_{\mathrm{gt2}}()$, RH() mainly involving the removal of lower-order inter-modulation components within $n \times F1 \pm m \times F2$, where n and m are integers less than 2. Finally, $\mathrm{NN_{P2}}$ is trained using $Z_{1\mathrm{fv}}$ and the GT to represent the NN network for P2, denoted as $\mathrm{NN_{P2}}$. The 'NN Engines' of P2 in figure 8 represent the training program modules used for training $\mathrm{NN_{p2}}$.

2) INFERENCE PHASE

$$\mathrm{Z_2} = \mathrm{NN_{P1}}(Y_{fv})\text{-}\mathrm{NN_{P2}}(Y - NN_{P1}(Y_{fv})) \quad (10)$$

In the inference phase, the signal is passed through an ADC to acquire Y. Following a sequential process involving two NN, the output is $\mathrm{Z_2}$, which serves as the ultimate corrected output. This procedure enables real-time distortion correction within the LNA amplifier.

C. TRAINING DATASET AND NN SYSTEM HYPER-PARAMETERS

In this paper, all the training samples used need to be obtained through the target LNA being tested, utilizing the testing platform constructed as shown in figure 2.For single-tone

TABLE 1. NN structure and hyper-parameters.

NN ITEM	P1	P2
Model	Linear regression	Linear regression
Algorithm	BP	BP
training algorithm	Levenberg-Marquardt	Levenberg-Marquardt
hidden layer	1	1
hidden layer neurons	6	3
activation functions	tansig	tansig
Input Layer dimension	12	10
Output Layer dimension	1	1
Input DelayStep1N	5	1
Input Interval_N	5	7
Input Interval	5	7
Input $\frac{\partial X_{in}(t)}{\partial t}$	1	1
Input $\frac{\partial^2 X_{in}(t)}{\partial^2 t}$	1	1

samples, signal source (1) was activated, while signal sources (2) and (3) were deactivated. For dual-tone samples, signal sources (1) and (2) were activated, while signal source (3) was deactivated. The mixed signals, after passing through the LNA, were collected to generate training samples. Subsequently, the GT data was obtained using the $F_{gt}()$ method mentioned earlier. The ADC sampling rate in this project is 125MHz, and the target frequency range is the shortwave band (3∼30MHz). Each sample consists of 16,384 sampling points.

While having a large number of samples can improve accuracy, it should be noted that different LC harmonic filters need to be replaced to suit different frequencies of Xin. This process can be time-consuming and labor-intensive when dealing with a large number of samples. To simplify the process of acquiring training samples and reduce costs, the goal was to obtain LNA distortion characteristics with as few training samples as possible. To achieve this, a well-planned approach for sample parameters was required. P1 and P2 have different requirements for training samples. For P1, the training was conducted in the frequency dimension, with one group of samples obtained every 2MHz in the frequency range from 3MHz to 15MHz and every 5MHz in the range from 15MHz to 30MHz. Each group of samples had four power levels for LNA input: −40dBm, −30dBm, −20dBm, and −10dBm, resulting in a total of 40 samples. On the other hand, P2 was trained with dual-tone samples, and 15 different dual-tone signals with equal amplitude were randomly combined within the 3∼30MHz frequency range.

A shallow-layer BP neural network was used for the NN in both P1 and P2. Below is the NN structure and system parameters in table 1. MATLAB's neural network toolbox was used.

V. EVALUATION OF PROPOSED CALIBRATION APPROACH

In this section, our proposed approach will be evaluation with the test system. The training and test results are presented as follows. The NN model employed was trained based on the parameters listed in table 1 and the training dataset discussed in the preceding sections. As shown in figure 10, the convergence performance curves for Part 1 and Part 2 are provided.

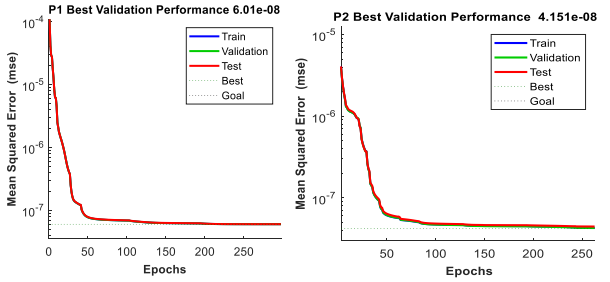

FIGURE 10. P1 (left)and P2(right) convergence curve of the training.

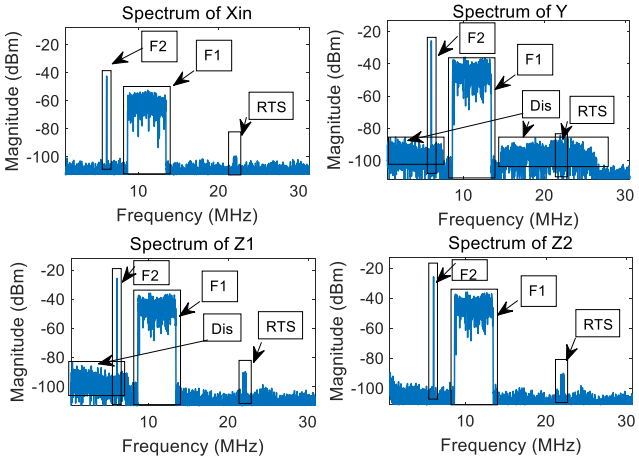

FIGURE 11. Spectra of X_{in}, Y, Z_1 and Z_2 with single and distortion (Dis).

A. EVALUATION METHODS AND TESTING FOR THE MODEL

Figure 2 illustrates the testing system, wherein signal sources (1) and (2) are used to generate test signals, both wideband and narrowband, identified as F1 and F2, for interference purposes. Additionally, a low-power multi-tone test signal known as RTS (Receive Target Signal) is produced by signal source (3). These signals are described as follows:

- F1: A white noise signal with a center frequency of 11 MHz and a bandwidth of 4 MHz
- F2: A single-tone strong signal with a center frequency of 6 MHz
- RTS: A low-power multi-tone test signal with a center frequency of 22 MHz and a bandwidth of 400 kHz.

F1, F2, and RTS signals are combined in Power Combiner to create the test signal X_{in}. The test signal is routed directly to the ADC, bypassing the LNA, to obtain X_{in}. The spectrum of X_{in} is plotted in figure 11. X_{in} passes through the LNA and is sampled by an ADC to obtain samples referred to as Y. The spectrum of Y is plotted in figure 11. Subsequently, the Y samples are processed by our proposed NN system to produce Z_2 after eliminating distortions, as plotted in figure 11.

TABLE 2. Test sample parameters.

	F1			F2			RST		
	Frq	Band	Pow	Frq	Band	Pow	Frq	Band	Pow
Test1	11	4	-38	6	--	-42	22	0.4	-95
Test2	10	4	-38	6	5	-42	22	0.4	-98
Test3	8	2	-43	6	--	-40	20	0.4	-98
Test4	9	--	-42	11	--	-42	22	0.4	-88
Test5	8	--	-21	--	--	--	--	--	--

Frq: Center frequency (MHz), Band: Bandwidth (MHz), Pow: Peak power (dBm)

In addition, the signal Z_1 is derived after the NN_{P1} processing phase, and its spectrum is plotted in figure 11.

Incorporating the system depicted in figure 2, a series of tests were conducted on the well-trained model, employing the previously mentioned testing methods. The test input parameter of X_{in} list in table 2. After passing through the LNA, the spectrum of the distorted signal Y and the spectrum of the output Z_2 after distortion mitigation by the model are compared, as shown in figure 12.

B. ANALYSIS OF EXPERIMENTAL RESULTS

When directly sampling X_{in} as shown in figure 12, the spectrum does not exhibit significant distortion. However, this setup results in a system with a higher noise figure, leading to a relatively lower signal-to-noise ratio (SNR) for received RST. This is the primary reason for the necessity of using an LNA at the system's front end. By incorporating an LNA at the front end, the lower noise figure and higher gain of the LNA significantly enhance the SNR of the SRT. However, the mixed signal X_{in}, after passing through the LNA, manifests noticeable harmonic and intermodulation distortions, as plotted in figure 12 (labeled as Y) and figure 12 (Tests, labeled as Y). The spectral components of the distortion affect a substantial portion of the frequency range. Although the intensity of these distortion components is not high, it is sufficient to overshadow the RST signal, despite being amplified by the LNA.

Signal Y is fed into a well-trained NN for inference. Upon completing the first part of the inference, Z_1 is obtained, as plotted in figure 12. As anticipated, the results align with our expectations. Harmonic and intermodulation distortions at frequencies higher than those of the F1 and F2 signals are significantly eliminated. Importantly, the RST signal remains unaffected, indicating that the NN_{P1} stage effectively eliminates the high-frequency harmonic and intermodulation distortions, rather than simply applying a low-pass filter. Z_1 undergoes NN_{P2} inference, ultimately yielding Z_2, as clearly shown in figure 12. Z_2 demonstrates the NN_{P2} successful eliminate low-frequency distortion components.

From experimental of test1 to test4 show in figure 12, it can be seen that when the input power is much lower than the input 1dB compression point (−19dbm) of the LNA,

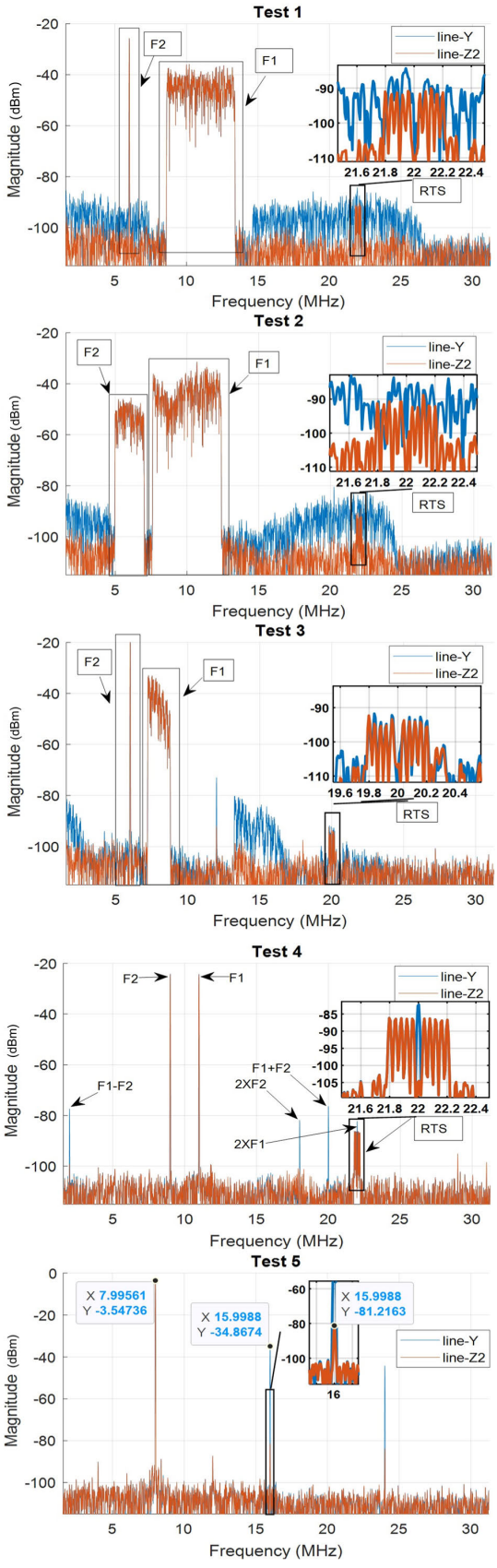

FIGURE 12. Test results of spectra of Y and Z2 with single and distortion.

TABLE 3. Comparison with prior works.

ITEM	Arch	Method	Rx_ref need	FBW (%)	Max SFDR/SNR /SNDR improve (dB)	distortion components reduce (dB)
This work	DSR	NN	**No**	160	**40 (SFDR)*** **30 (SNR)*** **30 (SNDR)***	**46 ***
[4]	DSR	Hammerstein	Need	108	N/A	25
[10]	DSR	LUT	No	N/A	7 (SNR)	40
[5]	DSR	polynomial	Need	10.5	20 (SFDR)	N/A
[14]	DCR	polynomial	Need	26.6	30 (SNR)	N/A
[15]	DSR	Hammerstein	No	200	20 (SFDR)	N/A
[16]	DSR	polynomial	Need	160	N/A	30
[26]	DCR	Hammerstein	Need	5.7	19 (SNDR)	N/A
[9]	DCR	polynomial	No	12.5	N/A	~26 (RF)
	* The max value obtained from the worst distorted channel					

our proposed method reduces the distortion caused by input signals to a level close to the quantization noise floor. In test 5 of figure 12, a relatively large single-tone input was utilized to assess the boundary performance of the system. The input brought the LNA close to the 1dB input compression point, and it can be observed that the improvement of the second harmonic distortion (HD2) is approximately 46dB, with the suppression of the third harmonic distortion (HD3) approaching 40dB.

Comparisons of several solutions with different methods are made, with some additional details shown in table 3. table 3 presents a comparison between the method proposed in this article and previous solutions. This method provides higher SFDR, improved SNR, and maximum distortion component elimination. It is important to note that during the testing process in this article, many distortion components were reduced to the noise floor, making it impossible to precisely quantify the extent of improvement. Therefore, in test5 of figure 12, a single-tone signal with a larger amplitude was used as the maximum capacity test, and the data obtained represents the maximum values achieved in this experiment. From figure 12 and table 3, it can be observed that the recommended method effectively eliminates the nonlinear distortions introduced by the RF front-end LNA without relying on auxiliary channels and with a large FBW. In comparison to traditional polynomial and adaptive filter methods, this approach demonstrates superior learning and approximation of the LNA's nonlinear distortion characteristics across a broader range. As a result, outstanding LNA linearization performance is achieved under high FBW conditions.

VI. CONCLUSION

In this paper, A method is introduced for eliminating nonlinear distortion in the LNA across multi-frequency bands using NN. The core concept of this method involves establishing an NN model to infer the non-linear distortion components generated by LNA devices under different stimuli, including various statistical distributions of frequency, power, and bandwidth. During the implementation of this method, two critical technological innovations, which include feature engineering based on the mathematical characteristics of signal effects on LNAs and Ground truth sets are acquired through a frequency-domain distortion separation method based on specialized training signals, have significantly reduced the complexity and training costs of the NN network. To validate the proposed method, a hardware platform was constructed, and tests were conducted using actual LNA devices. The results demonstrate that this method effectively eliminates intermodulation and harmonic distortion components caused by strong signals in a wide-frequency band, significantly enhancing the reception performance of high FBW MDSR. It is worth noting that this approach can be extended to applications in DPD, enabling an NN model of an amplifier to be adaptable across high FBW and multiple frequencies and power levels. This achievement holds significant potential for a wide range of applications.

REFERENCES

[1] T. Neu. (2015). *Direct RF Conversion: From Vision to Reality*. Texas Instrum. [Online]. Available: https://www.ti.com/jp/lit/pdf/slyy068
[2] T. Das. (2013). *Practical Considerations for Low Noise Amplifier Design*. Freescale Semiconductor. [Online]. Available: https://www.nxp.com/docs/en/white-paper/RFLNAWP.pdf
[3] R. Vansebrouck, O. Jamin, P. Desgreys, and V.-T. Nguyen, "Digital distortion compensation for wideband direct digitization RF receiver," in *Proc. IEEE 13th Int. New Circuits Syst. Conf. (NEWCAS)*, Grenoble, France, Jun. 2015, pp. 1–4, doi: 10.1109/NEWCAS.2015.7182109.
[4] N.-A. Vu, H.-N. Le, T.-H.-T. Tran, V.-P. Hoang, and Q.-K. Trinh, "Adaptive distortion inversion technique for LNA's nonlinearity compensation in direct RF digitization receivers," in *Proc. Int. Conf. Adv. Technol. Commun. (ATC)*, Hanoi, Vietnam, Oct. 2019, pp. 117–122, doi: 10.1109/ATC.2019.8924528.
[5] N.-A. Vu, T.-H.-T. Tran, H.-N. Le, H. D. Nguyen, and Q.-K. Trinh, "Undersampling reference receiver for LNA distortions compensation direct RF digitization receiver," in *Proc. 22th Int. Conf. Digit. Signal Process. Appl. (DSPA)*, Moscow, Russia, Mar. 2020, pp. 1–5, doi: 10.1109/DSPA48919.2020.9213283.
[6] L. Wang, J. Wang, J. Zhao, and J. Wu, "Line-element based nonlinear adaptive piecewise compensating correction for LVDT sensors," *J. Beijing Inst. Technol.*, vol. 22, no. 4, pp. 497–503, 2013.
[7] D. Chengxian, "Based-on nonlinear compensation self-tuning PID control," in *Proc. 3rd World Congr. Intell. Control Autom.*, vol. 5, Hefei, China, 2000, pp. 3104–3106, doi: 10.1109/wcica.2000.863032.
[8] W. Zhou, S. Yang, L. Wang, H. Sheng, and Y. Deng, "A nonlinear calibration method based on sinusoidal excitation and DFT transformation for high-precision power analyzers," *J. Sensors*, vol. 2021, pp. 1–9, Oct. 2021, doi: 10.1155/2021/5578361.
[9] M. Grimm, M. Allén, J. Marttila, M. Valkama, and R. Thomä, "Joint mitigation of nonlinear RF and baseband distortions in wideband direct-conversion receivers," *IEEE Trans. Microw. Theory Techn.*, vol. 62, no. 1, pp. 166–182, Jan. 2014, doi: 10.1109/TMTT.2013.2292603.
[10] N.-A. Vu, H.-N. Le, T.-H.-T. Tran, and Q.-K. Trinh, "A LUT-based scheme for LNA linearization in direct RF sampling receivers," *Phys. Commun.*, vol. 50, Feb. 2022, Art. no. 101530, doi: 10.1016/j.phycom.2021.101530.
[11] J. K. Cavers, "Amplifier linearization using a digital predistorter with fast adaptation and low memory requirements," *IEEE Trans. Veh. Technol.*, vol. 39, no. 4, pp. 374–382, Nov. 1990, doi: 10.1109/25.61359.
[12] H.-H. Chen, P.-C. Huang, C.-K. Wen, and J.-T. Chen, "Adaptive compensation of even-order distortion in direct conversion receivers," in *Proc. IEEE 58th Veh. Technol. Conf. (VTC-Fall)*, Orlando, FL, USA, Oct. 2003, pp. 271–274, doi: 10.1109/VETECF.2003.1285021.
[13] R. Gomez, H. Zou, B. Chen, B. Currivan, and D. Chang, "A full-band processor for reduction of RF mixer LO harmonic images," in *Proc. IEEE Custom Integr. Circuits Conf.*, San Jose, CA, USA, Sep. 2012, pp. 1–4, doi: 10.1109/CICC.2012.6330614.
[14] T.-H.-T. Tran, H.-N. Le, N.-A. Vu, N. P. Minh, T.-H. Nguyen, and Q.-K. Trinh, "LNA linearization solution for direct conversion receiver using under-sampling technique in reference receiver," *Phys. Commun.*, vol. 59, Aug. 2023, Art. no. 102059, doi: 10.1016/j.phycom.2023.102059.

[15] L. Peng and H. Ma, "Design and implementation of software-defined radio receiver based on blind nonlinear system identification and compensation," *IEEE Trans. Circuits Syst. I, Reg. Papers*, vol. 58, no. 11, pp. 2776–2789, Nov. 2011, doi: 10.1109/TCSI.2011.2151050.
[16] N.-A. Vu, T.-H.-T. Tran, Q.-K. Trinh, and H.-N. Le, "LNA nonlinear distortion impacts in multichannel direct RF digitization receivers and linearization techniques," in *Intelligent Computing in Engineering* (Advances in Intelligent Systems and Computing), vol. 1125. Singapore: Springer, 2020, pp. 1045–1053, doi: 10.1007/978-981-15-2780-7_109.
[17] L. Xie, H. Wei, and K. Zhang, "Behavioral modeling of nonlinear RF power amplifiers using ensemble SDBCC network," *Neurocomputing*, vol. 154, pp. 24–32, Apr. 2015, doi: 10.1016/j.neucom.2014.12.027.
[18] X. Hu, Z. Liu, X. Yu, Y. Zhao, W. Chen, B. Hu, X. Du, X. Li, M. Helaoui, W. Wang, and F. M. Ghannouchi, "Convolutional neural network for behavioral modeling and predistortion of wideband power amplifiers," *IEEE Trans. Neural Netw. Learn. Syst.*, vol. 33, no. 8, pp. 3923–3937, Aug. 2022, doi: 10.1109/TNNLS.2021.3054867.
[19] H. Wu, W. Chen, X. Liu, Z. Feng, and F. M. Ghannouchi, "A uniform neural network digital predistortion model of RF power amplifiers for scalable applications," *IEEE Trans. Microw. Theory Techn.*, vol. 70, no. 11, pp. 4885–4899, Nov. 2022, doi: 10.1109/TMTT.2022.3205930.
[20] P. Jaraut, A. Abdelhafiz, H. Chenini, X. Hu, M. Helaoui, M. Rawat, W. Chen, N. Boulejfen, and F. M. Ghannouchi, "Augmented convolutional neural network for behavioral modeling and digital predistortion of concurrent multiband power amplifiers," *IEEE Trans. Microw. Theory Techn.*, vol. 69, no. 9, pp. 4142–4156, Sep. 2021, doi: 10.1109/TMTT.2021.3075689.
[21] P. Jaraut, M. Rawat, and F. M. Ghannouchi, "Composite neural network digital predistortion model for joint mitigation of crosstalk, I/Q imbalance, nonlinearity in MIMO transmitters," *IEEE Trans. Microw. Theory Techn.*, vol. 66, no. 11, pp. 5011–5020, Nov. 2018, doi: 10.1109/TMTT.2018.2869602.
[22] C. Jiang, G. Yang, R. Han, J. Tan, and F. Liu, "Gated dynamic neural network model for digital predistortion of RF power amplifiers with varying transmission configurations," *IEEE Trans. Microw. Theory Techn.*, vol. 71, no. 8, pp. 3605–3616, Aug. 2023, doi: 10.1109/TMTT.2023.3241612.
[23] J. Steel and A. Parker, "Frequency-dependent distortion mechanism in a broadband amplifier," in *53rd ARFTG Conf. Dig.*, Anaheim, CA, USA, Jun. 1999, pp. 1–10, doi: 10.1109/arftg.1999.327329.
[24] M. Rafie, A. Abdipour, and G. Moradi, "Nonlinear distortion analysis of an amplifier, having a large number of nonlinear elements, using Volterra series," in *Proc. Int. Conf. Recent Adv. Microw. Theory Appl.*, Jaipur, India, Nov. 2008, pp. 939–942, doi: 10.1109/amta.2008.4763125.
[25] D. Zhai, W. Jiang, X. Jia, J. Lan, M. Guo, S.-W. Sin, F. Ye, Q. Liu, J. Ren, and C. Chen, "High-speed and time-interleaved ADCs using additive-neural-network-based calibration for nonlinear amplitude and phase distortion," *IEEE Trans. Circuits Syst. I, Reg. Papers*, vol. 69, no. 12, pp. 4944–4957, Dec. 2022, doi: 10.1109/TCSI.2022.3201016.
[26] J. Marttila, M. Allén, M. Kosunen, K. Stadius, J. Ryynänen, and M. Valkama, "Reference receiver enhanced digital linearization of wideband direct-conversion receivers," *IEEE Trans. Microw. Theory Techn.*, vol. 65, no. 2, pp. 607–620, Feb. 2017, doi: 10.1109/TMTT.2016.2638840.

ZHENG XIANG LI received the B.S. and M.S. degrees in communication and information systems from the Communication University of China, in 2006 and 2008, respectively. He is currently a Professor with the State Key Laboratory of Media Convergence and Communication, Communication University of China. His research interests include wireless communication and signal and information processing.

RUI LV received the Ph.D. degree from the National University of Defense Technology, in 1991. He was a Postdoctoral Researcher with Beijing Institute of Technology, from 1991 to 1993. He is currently the Director of the Xinhua News Agency Technical Expert Committee and the Director and a Doctoral Supervisor with the Engineering Research Center of Digital Audio and Video Ministry of Education, Communication University of China. His research interests include digital audio broadcasting, mobile multimedia broadcasting systems, digital audio and video technology, and real-time signal processing. He was the Vice President of the Communication University of China.